Available online at www.sciencedirect.com
SCIENCE DIRECT
Journal of Molecular Catalysis A: Chemical 241 (2005) 205–214
JOURNAL OF MOLECULAR CATALYSIS A: CHEMICAL
www.elsevier.com/locate/molcata

Synthesis, characterization and catalytic application of mesoporous W-MCM-48 for the selective oxidation of cyclopentene to glutaraldehyde

Xin-Li Yang [a], Wei-Lin Dai [a,*], Ruihua Gao [a], Hui Chen [a], Hexing Li [b], Yong Cao [a], Kangnian Fan [a,*]

[a] *Department of Chemistry and Shanghai Key Laboratory of Molecular Catalysis and Innovative Materials, Fudan University, Shanghai 200433, PR China*
[b] *Department of Chemistry, Shanghai Normal University, Shanghai 200234, PR China*

Received 18 February 2005; received in revised form 16 July 2005; accepted 19 July 2005
Available online 22 August 2005

Abstract

Tungsten-containing ordered MCM-48 has been synthesized under hydrothermal conditions via pH adjustment and characterized with various analytical and spectroscopic techniques including X-ray diffraction (XRD), N_2 adsorption, transmission electron micrographs (TEM), scanning electron micrographs (SEM), Laser-Raman spectroscopy, UV–vis diffuse reflectance spectroscopy (UV–vis DRS), Fourier-transform infrared spectroscopy (FT-IR) and ammonia temperature-programmed desorption (NH_3-TPD). XRD and FT-IR results indicate that the substitution of tungsten occurs in the silicate framework structure of MCM-48. TEM and SEM investigations confirm the presence of ordered cubic structure in the novel W-MCM-48 material. NH_3-TPD and FT-IR-pyridine adsorption experiments indicate that the strong Brønsted and Lewis acid sites are formed upon incorporation of tungsten in the mesoporous MCM48 framework and the moderately strong acidity of the W-MCM-48 catalyst is beneficial to its good catalytic performance. The as-synthesized W-MCM-48 material is very active as a heterogeneous catalyst for the selective oxidation of cyclopentene (CPE) to glutaraldehyde (GA) with environmentally benign aqueous hydrogen peroxide as the oxidant. Tungsten species could stably exist in the silica-based matrix of MCM-48 up to WO_3 content of 20 wt%. Both the proper content of tungsten species and its high dispersion account for its high activity. The 20 wt% W-MCM-48 catalyst shows CPE conversion of 85.2% and GA yield of 66.9%, respectively. Furthermore, almost no tungsten species are leached into the reaction solution, enabling the catalyst to be a promising candidate for its further application in industry.

Keywords: Cyclopentene; Glutaraldehyde; H_2O_2; Tungsten; MCM-48; W-MCM-48

1. Introduction

Since the first invention of M41S by the Mobil researchers, a series of mesoporous materials with pore dimensions larger than 20 Å have been synthesized using structure-directing templates [1]. The M41S series include hexagonal MCM-41 and cubic MCM-48, all characteristic with a very large surface area and abundant porosity as well as long-range ordered pore structure [2,3]. During the last decade, these materials have attracted much research interest because of their potential application in catalysis [4], sorption [5] and synthesis of fine chemicals [6], since their pores are larger than those of microporous molecular sieves, then allowing a faster diffusion and processing of bulky molecules. However, it is noteworthy that particular attention has been paid to one-dimensional MCM-41 and much less attention has been paid to the three-dimensional mesoporous MCM-48, mainly due to its difficulty in synthesis [7,8]. In addition, the cubic MCM-48 is promising from the point of view of its potential application in practical industry owing to the resistance to pore blocking. As a result, it entails more agitated flow, which then increases the interaction possibility between reactants and catalytic active centers. Thus, considerable efforts have been made till now in the optimization of

* Corresponding authors. Fax: +86 21 65642978.
E-mail addresses: wldai@fudan.edu.cn (W.-L. Dai), knfan@fudan.edu.cn (K. Fan).

1381-1169/$ – see front matter © 2005 Elsevier B.V. All rights reserved.
doi:10.1016/j.molcata.2005.07.025

the synthesis parameters and catalytic applications of MCM-48-based material with satisfactory results [9–21].

However, the pure silica mesoporous M41S materials possess a neutral framework, which limits their applications in catalysis, sorption, molecular sieving, supports, etc. In order to provide this material with potential catalytic applications, it is possible, like for zeolites, to modify the nature of the framework by incorporation of hetero-elements. Hence, various transition elements including tungsten have been incorporated into the framework of MCM-41 and the resulting systems are active for many catalytic reactions [22–24]. Up to now, attempts to incorporate Al [25–28], Mn [27,29], Fe [30], Zr [31], Ti [32–36], B [37] and V [38,39] into MCM-48 have already been reported. However, little attention is paid to the synthesis and characterization as well as the catalytic application of tungsten-containing MCM-48 [40,41].

In view of the importance of MCM-48 structure as well as its possible application as a good support in catalysis, tungsten has been chosen as the hetero-element to synthesize W-MCM-48 mesoporous material in the present work, which was synthesized through the in situ method with different weight percents (5–30%) of tungsten oxide, and were then characterized with various techniques including XRD, N_2 sorption, TEM, SEM, Laser-Raman, FT-IR and NH_3-TPD. In addition, the catalytic performance of the as-synthesized W-MCM-48 material was investigated toward the selective oxidation of cyclopentene (CPE) to glutaraldehyde (GA) that has been used extensively for disinfection and sterilization in many areas. However, the commercial preparation method from propenal and vinyl ethyl ether is now being restricted by its complicated preparation process and expensive raw materials [42,43], resulting in the high price of GA and has constrained its wide use in other fields, such as the tanning process of leather and water treatment. The preparation of GA in a more convenient and economical way has been an important objective for many researchers. An alternative way to produce GA is the selective oxidation of CPE with environmentally benign aqueous H_2O_2 as the green oxidant, since a great quantity of CPE could be easily obtained by the selective hydrogenation of cyclopentadiene (CPD). The direct synthesis of GA from CPE appears to be an attractive way of utilizing dicyclopentadiene (DCPD), a main by-product of the C-5 fraction in the petrochemical industry [44,45].

2. Experimental

2.1. Catalyst preparation

A series of tungsten-containing MCM-48 samples were synthesized under hydrothermal conditions via pH adjustment according to the following procedure. Firstly, a solution of cetyltrimethylammonium bromide (CTAB) and NaOH was added to the aqueous sodium tungstate solution ($Na_2WO_4{\cdot}2H_2O$, 0.2 M) and the mixture was stirred for 30 min. Then, tetraethyl orthosilicate (TEOS) was added to the above mixture under vigorous stirring. The resulting gel was stirred for 2 h and transferred into a teflon-lined stainless steel autoclave and kept in an air oven at 368 K for 72 h while the pH value of the gel was adjusted to ca. 2 with hydrochloric acid. Then, the autoclaves were sealed and kept in an air oven at 368 K for 24 h. The precipitate was obtained by filtration, and was then washed with distilled water, dried at 368 K for 24 h and finally calcined at 873 K in air for 5 h. The as-obtained gel had a chemical (molar) composition of $1SiO_2$:0.48CTAB:0.48NaOH:$55H_2O$:xWO_3 ($x = 0.0125$–0.1). The pure silica MCM-48 was synthesized in a similar manner to the above process only by omitting the procedure of $Na_2WO_4{\cdot}2H_2O$ addition and the pH adjustment. For the purpose of comparison, the WO_3-supported catalyst was prepared through the conventional incipient wetness impregnation method as follows. The required amount of tungstic acid, $WO_3{\cdot}H_2O$, was dissolved in an aqueous solution of ammonia. Into the stirred solution was dispersed pure MCM-48 or commercial silica at 353 K. After the excess water was evaporated completely, the WO_3/MCM-48 or WO_3/SiO_2 catalyst was then obtained after the dried solids were further calcined at 873 K in air for 3 h.

2.2. Catalyst characterization

The low-angle X-ray powder diffraction patterns were recorded on a Rigaku D/max-rB spectrometer with Cu Kα radiation, which was operated at 60 mA and 40 kV. The wide-angle X-ray powder diffraction patterns were recorded on a Bruker D8 advance spectrometer with Cu Kα radiation, which was operated at 40 mA and 40 kV. The Laser-Raman experiment was performed by using a Jobin Yvon Dilor Labram I Raman spectrometer equipped with a holographic notch filter, a CCD detector and a He–Ne laser radiating at 632.8 nm. The specific surface areas, the pore volumes and the mean pore diameters of the samples were measured and calculated according to the BET method with a Micromeritics Tristar ASAP3000 BET apparatus with liquid nitrogen at 77 K. Scanning electron micrographs were obtained using a Philips XL 30 electron microscope. The samples were deposited on a sample holder with a piece of adhesive carbon tape and were then sputtered with a thin film of gold. Transmission electron micrographs were obtained on a JOEL JEM 2010 scan-transmission electron microscope. The samples were supported on carbon-coated copper grids for the experiment. UV–vis diffuse reflectance spectra were collected on a Shimadzu UV-2540 spectrometer with $BaSO_4$ as a reference. The FT-IR measurements were carried out with a Nicolet Model 205 spectrometer using the KBr pellet technique. The surface acidity was monitored from the FT-IR spectra recorded after the adsorption of pyridine, using a Bruker Vector 22 spectrometer coupled to a conventional high vacuum system. The sample was compacted to a self-supporting wafer and was calcined at 673 K for 1 h in an in situ IR gas cell under vacuum prior to pyridine adsorption [46]. Pyridine was adsorbed at room temperature from an argon flow

containing 2 vol% pyridine. Then, the samples were heated to 373 K and evacuated to remove physisorbed and weakly chemisorbed pyridine. Temperature-programmed desorption of the adsorbed pyridine starting at 373 K was studied by stepwise heating of the sample under vacuum to characterize the kinds and strength of the acid sites. Difference spectra were obtained by subtracting the background (base spectrum) of the unloaded sample. The NH_3-TPD experiments were conducted on a home built flow apparatus. Prior to TPD experiment, the sample was pretreated with high-purity (99.999%) helium (30 mL/min) at 773 K for 2 h. After pretreatment, the sample was saturated with high purity anhydrous ammonia from 10% NH_3 and balance He mixture (30 mL/min) at 393 K for 1 h and subsequently flushed at 393 K for 2 h to remove physisorbed ammonia. TPD experiment was carried out from 393 to 873 K at a heating rate of 10 K/min. The amount of desorbed NH_3 was calculated using CDMC software accompanied with the GC workstation. The tungsten content in W-MCM-48 was determined by inductively coupled argon plasma (ICP, IRIS Intrepid, Thermo Elemental Company) after solubilization of the samples in HF:HCl solutions.

2.3. Activity test

The activity test was performed at 308 K for 35–44 h with magnetic stirring in a closed 100 mL regular glass reactor using 50 wt% aqueous H_2O_2 as oxygen-donor and *t*-BuOH as the solvent. In a typical experiment, 5 mL of CPE, 50 mL of *t*-BuOH and 0.6 g of the W-MCM-48 (20 wt%) were introduced into the regular glass reactor at 308 K with vigorous stirring. The reaction was started by adding 7 mL of 50 wt% aqueous H_2O_2 into the mixture and was kept for 35–44 h. The quantitative analysis of the reaction products was done by the GC method and the determination of different products in the reaction mixture was performed by means of GC–MS. Details can be found in our previous work elsewhere [47].

3. Results and discussion

The small-angle powder XRD patterns of W-containing MCM-48 samples with different tungsten contents are shown in Fig. 1. The W-containing MCM-48 materials with WO_3 contents lower than 20 wt% exhibit a high intensity (2 1 1) peak followed by a smaller (2 0 0) one in the 2θ range of 2–3°, whereas several other peaks are observed in the 3–6° range, which corresponds to the *Ia*3*d* cubic symmetry reported for MCM-48 type molecular sieves [1,2]. Further increase in the WO_3 content up to 30% will lead to the partial collapse of the mesoporous structure. The supported one, WO_3/MCM-48 (20 wt%), prepared through the incipient wetness impregnation method with tungstic acid as the starting material also displays an reflection corresponding to the (2 1 1) plane; however, the intensity of the peak is very weak and other planes could not be easily observed. This is a clear indication that the W-containing MCM-48 catalyst prepared through the direct hydrothermal synthesis method shows much more uniform mesoporous structure than the conventional supported one. The unit cell parameters calculated from the (2 1 1) line, a_0, for all samples are also given in Table 1. It is obvious to find that an increment in the a_0 value is observed for W-MCM-48 as compared to its pure siliceously analogue. The shift in the reflections or the deviations of the a_0 values of as-prepared W-MCM-48 from pure MCM-48 can be ascribed to the atomic radius of W^{6+} (0.68 Å) being larger than that of Si^{4+} (0.40 Å) as well as to the W–O bond length being longer than that of Si–O. Similar results have been reported for V-containing

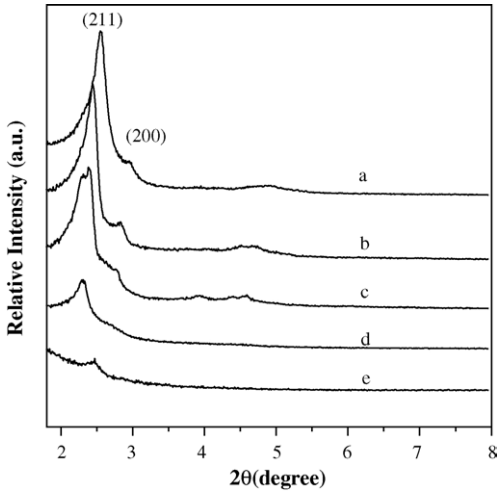

Fig. 1. Small-angle XRD patterns of various samples: (a) 5 wt%; (b) 10 wt%; (c) 20 wt%; (d) 30 wt% W-MCM-48; (e) 20 wt% WO_3/MCM-48.

Table 1
Physico-chemical parameters of various samples

Samples	Si/W[a] (mol)	Si/W[b] (mol)	Surface area (m^2/g)	Pore volume (cm^3/g)	Pore diameter (nm)	a_0[c] (nm)
Pure MCM-48	–	–	1159	1.38	1.4	8.9
5% W-MCM-48	77.2	122.5	876	1.15	2.6	9.2
10% W-MCM-48	38.6	70.1	752	1.12	2.5	9.6
20% W-MCM-48	19.3	38.5	635	1.08	2.4	10.2
30% W-MCM-48	12.8	17.8	396	0.70	2.3	10.5
20% WO_3/MCM-48	19.3	22.6	624	0.80	4.2	11.9

[a] Stoichiometric ratio in gel.
[b] Measured by ICP.
[c] $a_0 = d\{2\,1\,1\}/\sqrt{(h^2+k^2+l^2)}$.

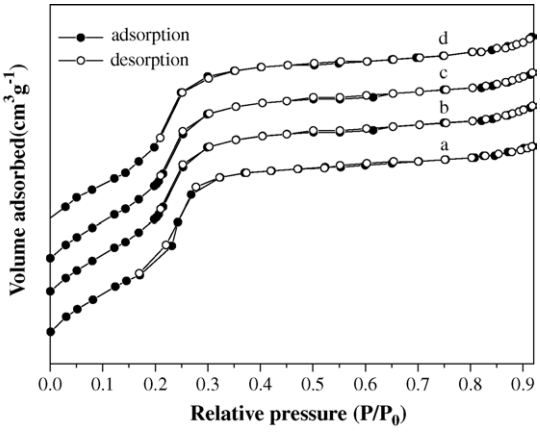

Fig. 2. Low temperature nitrogen adsorption–desorption isotherms of W-MCM-48 mesoporous materials: (a) 5 wt%; (b) 10 wt%; (c) 20 wt%; (d) 30 wt% W-MCM-48.

MCM-48 materials [48–50]. These differences verify possible substitution of tungsten ions into the silicate framework of MCM-48.

N_2 adsorption–desorption curves of W-MCM-48 samples show reversible type IV isotherms (see Fig. 2), also typical indication of mesoporous materials [51]. A sharp inflection observed from $P/P_0 = 0.2$–0.4 corresponds to typical capillary condensation with regular mesopores. On the other hand, the inflection also verifies the absence of any micropores filling at low P/P_0. Furthermore, no defined hysteresis loop was obtained in the adsorption and desorption cycle upon pore condensation, which was another character for MCM-48 materials. The pore volumes, surface areas and pore diameters obtained from N_2 sorption isotherms for all samples are also listed in Table 1. The BET surface area, pore volume as well as the pore diameter of W-MCM-48 samples are lower or higher than those of pure MCM-48, indicating the great influence of the incorporated hetero-atoms. Table 1 also lists the actual metal amounts in the products measured by the ICP method. It can be seen from Table 1 that the calcined samples have a deficiency of tungsten in comparison with the tungsten content added in the as-synthesized gel. This observation may be due to the fact that tungsten partly remained as soluble hydroxide in the mother liquor under post-synthesis conditions, and that it is removed during filtration and washing treatment, therefore giving a lower tungsten content in the calcined samples.

Typical morphology of 20 wt% W-MCM-48 is observed through SEM and TEM photos, as can be seen in Fig. 3. The 20 wt% W-MCM-48 sample retains the morphology and cubic-type ordering structure on the (1 1 0) cubic plane similar to those of pure MCM-48 [52], obviously indicating that WO_3 content of 20 wt% does not change its typical morphology. TEM analysis also reveals that no obvious extra phases of the WO_3 species are present outside of the mesoporous structure.

The Raman spectra of the as-prepared samples, as shown in Fig. 4, provide additional information about the WO_3 structure in the W-MCM-48 samples. In comparison with the standard octahedral crystalline WO_3 (Fig. 4(a)), no Raman bands attributed to the octahedral crystalline WO_3, at ca. 804, 714, 327 and 267 cm^{-1} [53] are observed for W-MCM-48 ($WO_3 \leq 20$ wt%, see Fig. 4(d and e)). The Raman bands in Fig. 4(d and e) are very similar to those of the pure MCM-48 (not shown here). Fig. 5(b) shows the Raman spectra of W-MCM-48 samples with a much higher content of tungsten

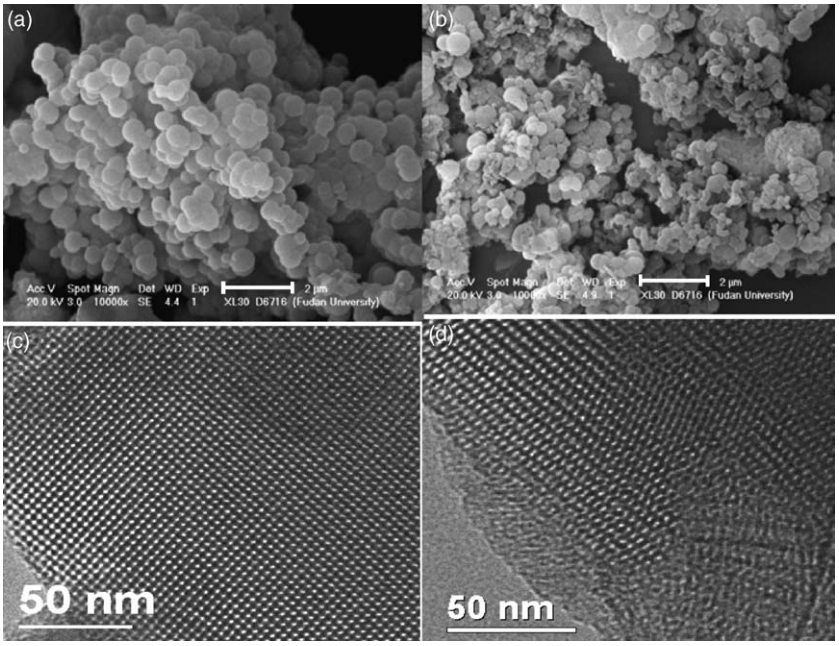

Fig. 3. SEM/TEM photos of pure and 20 wt% W-MCM-48 material. SEM photos of pure (a) and W-MCM-48 (b); TEM photos of pure (c) and W-MCM-48 (d).

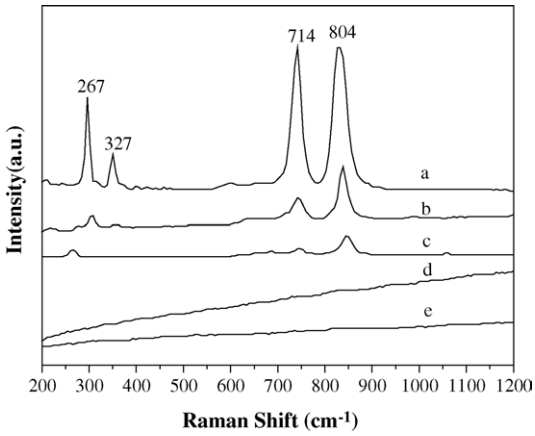

Fig. 4. Raman spectra of various samples: (a) WO_3 crystalline; (b) 30 wt% W-MCM-48; (c) 20 wt% WO_3/MCM-18; (d) 20 wt% W-MCM-48; (e) 10 wt% W-MCM-48.

species (ca. 30 wt%), where typical Raman bands assigned to crystalline WO_3 can be easily observed, illustrating that certain high contents of tungsten species would result in the agglomeration of microcrystalline WO_3 on the surface. Hence, a proper content of tungsten species is necessary for its high dispersion and the stability of special mesoporous structure of MCM-48. Fig. 4 also shows the Raman spectra of 20 wt% WO_3/MCM-48 (Fig. 4(c)) catalyst for comparison. Similarly, obvious Raman bands assigned to crystalline WO_3 can be observed for the supported catalyst, while the in situ synthesized 20 wt% counterpart presents no Raman bands of WO_3, suggesting that the WO_3 species are well dispersed in MCM-48 material for the in situ synthesized method, which is in line with the result from wide-angle XRD (not shown here).

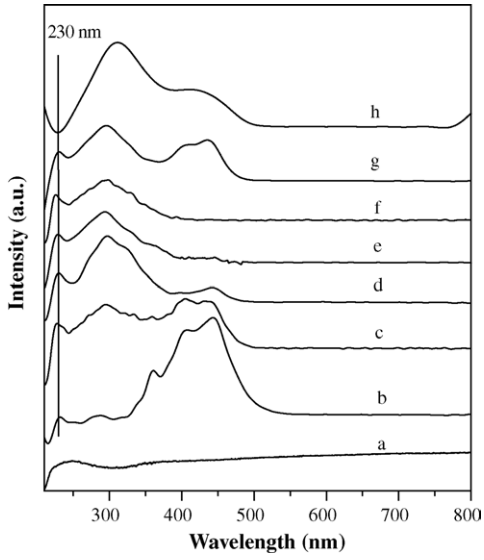

Fig. 5. UV–vis diffuse reflectance spectra of various samples after dehydration at 523 K in air for 2 h: (a) Si-MCM-48; (b) bulk WO_3; (c) 30 wt%; (d) 20 wt%; (e) 10 wt%; (f) 5 wt% W-MCM-48; (g) 20 wt% WO_3/MCM-48; (h) 20 wt% WO_3/SiO_2.

Since the Raman spectra demonstrate that parts of tungsten oxide species are incorporated into the MCM-48 framework, further investigation has been done by applying UV–vis diffuse reflectance spectroscopy. This method is well known to be very sensitive to distinguishing between incorporated metal species and extra framework metal oxides in different mesostructures [54,55]. The UV–vis DRS spectra of the 20 wt% W-MCM-48, WO_3/MCM-48 and WO_3/SiO_2 samples, as well as that of bulk WO_3 are presented in Fig. 5. For pure siliceous MCM-48, there are no evident bands in the spectrum (curve a). After tungsten oxide is introduced into MCM-48, three types of Raman bands at 230, 300 and 450 nm appear. The broad one at about 450 nm of 30% W-MCM-48 and the impregnated samples (curve c, g and h) can be attributed to tungsten trioxide by comparison with the spectrum of bulk WO_3 (curve b) [56,57]. The second broad band from 250 to 350 nm presents another kind of tungsten oxide species. The previous work of Weber and Iglesia et al. shows that the low-energy absorption is shifted towards lower wavelengths when the nuclearity of molybdenum or tungsten entities decreases [57–59]. Therefore, this broad band should be assigned to isolated tungsten species or low condensed oligomeric tungsten oxide species. The sharp band at 230 nm of the in situ synthesized samples (curve c–f) can be attributed to isolated $[WO_4]$ tetrahedral species by comparison of the structure of sodium tungstate ($Na_2WO_4{\cdot}H_2O$, not shown here) with the spinel structure and isolated $[WO_4]^{2-}$ tetrahedral [56,60]. The absence of the broad band at 450 nm may reflect that the tungsten oxide species are highly dispersed and no crystalline WO_3 is formed in W-MCM-48 samples with tungsten oxide contents lower than 20 wt% (curve e and f). There is a weak band at 450 nm for the 20 wt% W-MCM-48, which cannot be detected with Raman spectroscopy yet. Further increasing the tungsten oxide content up to 30 wt% will lead to the formation of crystalline WO_3, resulting in the appearance of strong bands at 450 nm confirmed by the Raman spectra and crystalline phase of WO_3 detected by XRD. The UV–vis DRS spectra further demonstrate that high dispersion of the tungsten oxide species is essential to the high catalytic performance of the as-synthesized catalysts as discussed below.

The FT-IR spectra of the W-containing samples are shown in Fig. 6. All the samples exhibit the symmetric and the anti-symmetric stretching vibration bands at around 460, 810 and 1100 cm^{-1} for the tetrahedral SiO_4 structure units. The band at 630 cm^{-1} is assigned to anti-symmetric stretching of O–W–O vibrations [61]. Generally, the band at around 960 cm^{-1} is assigned to Si–OH stretching vibrations in the calcined samples [62], however, which can also be assigned to the Si–O–W groups [63,64]. Furthermore, the intensity of the 960 cm^{-1} band enhances with an increase in the tungsten content in the W-MCM-48 samples, which could be attributed to the presence of non-extractable Si–O–W linkage in the mesoporous matrix.

Temperature-programmed desorption of probe molecules like ammonia and pyridine is a popular method for the

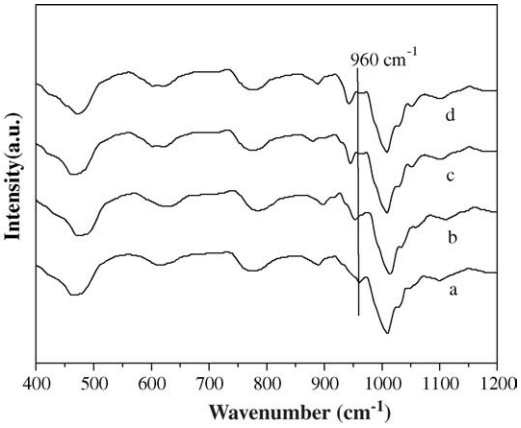

Fig. 6. FT-IR spectra of W-MCM-48 with different WO_3 contents: (a) 5 wt%; (b) 10 wt%; (c) 20 wt%; (d) 30 wt% W-MCM-48.

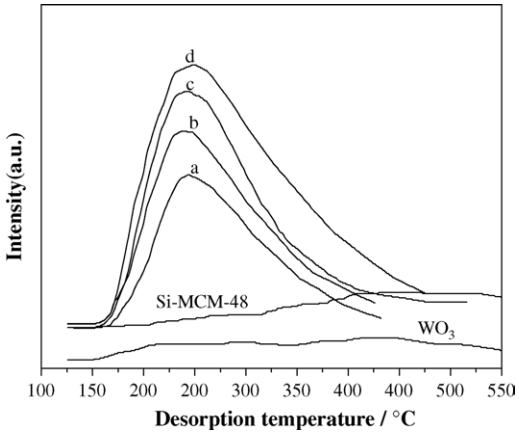

Fig. 7. NH_3-TPD profiles of various samples: (a) 5 wt% W-MCM-48; (b) 10 wt% W-MCM-48; (c) 20 wt% W-MCM-48; (d) 30 wt% W-MCM-48.

determination of acidity amount of solid catalysts as well as acid strength [65]. In the present investigation, the acidity measurements are carried out with the ammonia TPD method. It is well known that tungsten trioxide possesses Lewis acid sites [66]. If porous materials contain deposited tungsten oxide species, acid centers will be generated and ammonia adsorption–desorption effects could be observed. The NH_3-TPD profiles of the W-MCM-48 samples are present in Fig. 7. The acidity values and TPD peak temperature positions are given in Table 2. As expected, pure silica MCM-48 shows a little amount of ammonia desorption due to the lack of acid centers. On the other hand, there appears a broad peak of ammonia desorption as the transition metal tungsten is

Table 2
Summary of NH_3-TPD data upon W-MCM-48 catalysts

Samples	T_d (°C)	Acidic amounts (mmol NH_3/g)
Si-MCM-48	–	0.085
5% W-MCM-48	241	0.254
10% W-MCM-48	243	0.327
20% W-MCM-48	249	0.456
30% W-MCM-48	252	0.624

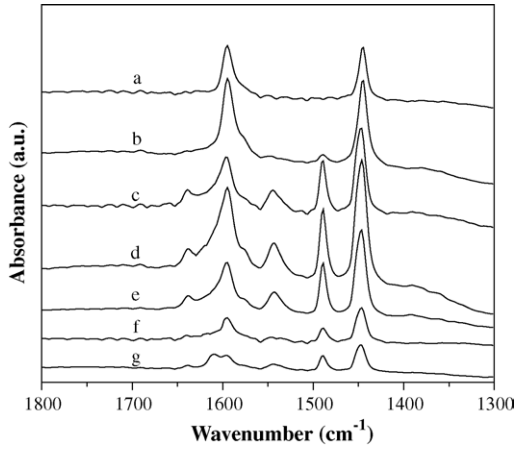

Fig. 8. FT-IR spectra of pyridine adsorbed on the sample: (a) MCM-48; (b) 5 wt%; (c) 10 wt%; (d) 20 wt%; (e) 30 wt% W-MCM-48; (f) 20 wt% WO_3/MCM-48; (g) 20 wt% WO_3/SiO_2.

incorporated into the bulk of MCM-48. Moreover, the acidity value increases and the desorption temperature shifts to a higher position, indicating acidity increases with the increase in the tungsten content in the W-MCM-48 samples. However, the value of CPE conversion during the selective oxidation of CPE to GA is found to decrease over the catalyst at 30 wt% of tungsten trioxide contents, indicating too much acidity is not beneficial to the target reaction.

Pyridine adsorption is followed by infrared spectroscopy to further identify the number and nature of acid sites on the surface of various samples. Fig. 8 shows the FT-IR spectra of the catalysts recorded after the adsorption of pyridine and subsequent evacuation at 423 K. The type of the acid sites and the vibrational modes of pyridine are summarized in Table 3 according to the reference [67]. For the pure MCM-48, only two bands at 1445 and 1595 cm^{-1} can be observed, corresponding to pyridine coordinately bond to weak surface Lewis acid sites [68]. When the out-gassing temperature is increased from 423 to 473 K, these peaks disappear. After tungsten species are incorporated into the framework of MCM-48, three new bands appear at 1488, 1545 and 1635 cm^{-1}, which are assigned to the formation

Table 3
The position of the FT-IR bands recorded after adsorption of pyridine onto the catalysts

Sample	B_{py}[a]			L_{py}[a]	
	8a	19a	19b	8a	19b
Si-MCM-48	–	–	–	1595	1445
5% W-MCM-48	1635	1488	1545	1595	1445
10% W-MCM-48	1635	1488	1545	1595	1445
20% W-MCM-48	1635	1488	1545	1595	1445
30% W-MCM-48	1635	1488	1545	1595	1445
20% WO_3/MCM-48	1635	1488	1545	1595	1445
20% WO_3/SiO_2	1635	1488	1545	1595	1445

[a] B_{py} (L_{py}) are the modes corresponding to pyridine adsorbed onto Brønsted (Lewis) acid sites; 8a, 19a and 19b are vibration modes of the pyridine molecule.

Table 4
Catalytic performance of the selective oxidation of CPE over various W-MCM-48 catalysts[a]

Catalysts	H_2O_2 conversion (%)	H_2O_2 efficiency[b] (%)	CPE conversion (%)	TOF (h^{-1})	Selectivity (%)			
					CPO	GA	CPLE	CPDL
WO_3	0.1	–	1.5	–	0	0	-	-
MCM-48	0	0	0	0	0	0	0	0
5% W-MCM-48	93.1	59.7	62.4	2.35	0.8	78.2	9.6	11.4
10% W-MCM-48	95.6	71.3	75.8	2.85	0.6	79.8	8.8	10.8
20% W-MCM-48	98.9	76.9	85.2	3.21	1.1	78.5	8.7	11.7
30% W-MCM-48	99.5	68.6	76.6	2.88	1.0	78.2	8.0	12.8
20% WO_3/MCM-48[c]	99.3	73.9	81.8	2.45	0.6	79.8	8.8	10.4
20% WO_3/SiO_2	65.2	59.4	50.2	1.89	11.4	60.8	9.7	11.7

[a] Reaction conditions: 5 mL cyclopentene, 7 mL 50% H_2O_2, 50 mL *t*-BuOH, 0.1 g WO_3, T = 308 K, reaction time 35 h; CPE, cyclopentene; CPO, cyclopentene-epoxide; GA, glutaraldehyde; CPDL, cyclopentan-1,2-diol; CPLE, 2-*t*-butyloxy-1-cyclopentanol.
[b] H_2O_2 efficiency: the number of moles H_2O_2 consumed to produce the products/the number of moles H_2O_2 converted.
[c] Reaction time 44 h.

of pyridinium ions at surface Brønsted acid sites, as shown in Fig. 8(b–e). It can also be found that the number of the Lewis and Brønsted acid sites increases with the tungsten oxide contents up to 20 wt%. In addition, for the 20 wt% W-MCM-48 catalyst, the intensities of these bands decrease, but are still recorded after out-gassing at 573 K thus indicating the presence of rather strong acid sites. While the number of the Lewis and Brønsted acid sites slightly decreases for the 30 wt% W-MCM-48, which may be caused by the weak interaction between the tungsten species and the silica because high contents of tungsten species may lead to the partial collapse of the mesoporous structure and the appearance of crystalline WO_3. However, the total amount of the acidity does not decease on the catalysts with much higher contents of tungsten species as shown in profiles of NH_3-TPD. For the purpose of comparison, Fig. 8 also gives the FT-IR spectra of the 20 wt% WO_3/MCM-48 and WO_3/SiO_2 catalysts prepared by the impregnation method. Obviously, the number of the Lewis and Brønsted acid sites of these catalysts is less than that of 20 wt% W-MCM-48 prepared by the in situ method. According to the FT-IR spectra after pyridine adsorption, it can be concluded that both the Lewis and Brønsted acid sites evidenced over the W-MCM-48 catalysts are related to tungsten oxide incorporation and that the strong Lewis and Brønsted acid sites are essential to the selective oxidation of CPE.

The catalytic performance over various W-containing catalysts with different tungsten contents is shown in Table 4. As shown in Table 4, the pure MCM-48 catalyst shows no transformation of CPE to GA. Furthermore, unsupported crystalline WO_3 shows little activity towards the title reaction, while those well-dispersed WO_3 on/in MCM-48 supports show substantial activity and selectivity to the cleavage reaction. This result suggests that the WO_3 species incorporated into the uniform framework of mesoporous MCM-48 materials act as the active centers for the selective oxidation of CPE. The TOF values (also shown in Table 4) unambiguously verified the above conclusion. It is also found that both the tungsten oxide content and the preparation method influence the catalytic performance intensively. W-MCM-48 catalysts show higher activity and selectivity than WO_3/MCM-48 and WO_3/SiO_2 analogues, indicating the in situ synthesized method for the preparation of W-MCM-48 is more beneficial to the well dispersion of active tungsten species than the incipient wetness impregnation one. When the WO_3 content is lower than 20%, low yield of GA is reached. However, if the WO_3 content is more than 20%, inevitable agglomeration of WO_3, the partial collapse of the mesoporous structure and the excess amount of strong acidity of the W-MCM-48 all lead not only to the lower CPE conversion but also to the lower GA yield. The 20 wt% W-MCM-48 catalyst shows 85.2% CPE conversion and 66.9% GA yield, a little higher than the previously reported in this reaction system by using WO_3/SiO_2 or WO_3/TiO_2-SiO_2 as catalysts [47,69]. The great differences in the catalytic performance among those W-MCM-48 catalysts with different tungsten contents suggest that the presence of the highly dispersed tungsten oxide species in the silica matrix is necessary for the selective oxidation of CPE to GA with aqueous H_2O_2 as the oxygen donor.

Investigation by means of UV–vis DRS has proved that, at low tungsten oxide contents (below 20 wt%), the W-MCM-48 samples possess isolated tungsten or low condensed tungsten species, which are highly dispersed into the framework of MCM-48. The highly dispersed tungsten oxide species may be responsible for the good performance of the catalysts. At a higher tungsten oxide content (30 wt%), crystalline tungsten trioxide appeared on the surface of the sample and was also detected by Raman spectroscopy, leading to the decrease in the catalytic activity. Only low condensed tungsten species and crystalline trioxide are present in the impregnated samples (WO_3/MCM-48 and WO_3/SiO_2), which results in their lower catalytic performance.

Characterization by FT-IR-pyridine adsorption has confirmed that strong Brønsted acid sites are formed by incorporating tungsten oxide species into the MCM-48 materials, which are still present even after out-gassing at 573 K (20% W-MCM-48). The number of Lewis acid sites is also enhanced, indicating both Brønsted acid sites and Lewis acid

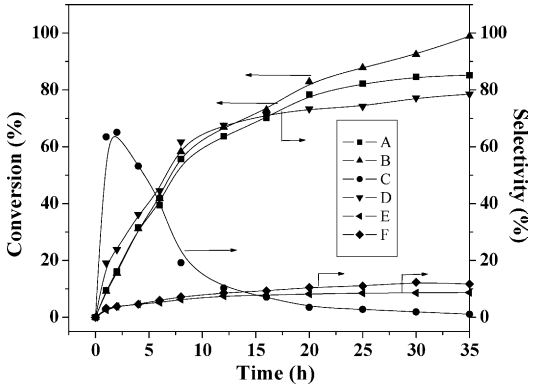

Fig. 9. Dependence of conversion of CPE and H_2O_2 and selectivity to GA, CPO, CPDL and CPLE on the reaction time. A = CPE, B = H_2O_2, C = CPO, D = GA, E = CPLE and F = CPDL.

sites are related to the improvement in the catalytic performance of the in situ synthesized samples.

According to the result of GC–MS analysis, besides GA as the main product, a variety of by-products such as cyclopentene oxide (CPO), cyclopentan-1,2-diol and 2-*t*-butyloxy-1-cyclopentanol are identified, indicating that the reaction is very complex in which different oxidation routes could exist. In order to explain the possible mechanism, the dependence of the CPE and H_2O_2 conversion as well as the selectivity towards GA and various by-products on the reaction time has been determined over 20 wt% W-MCM-48 catalyst as shown in Fig. 9. One can see that CPO is produced rapidly at the beginning and consumed progressively with the increase in GA, indicating that CPO is possibly a main intermediate from which GA is produced via its further oxidative cleavage. Moreover, the conversion of H_2O_2 is higher than that of CPE, indicating H_2O_2 is not efficiently used in the target reaction over the catalyst. As summarized in Table 4, the efficiency of H_2O_2 increases with the tungsten oxide content up to 20 wt% and decreases with further increment in WO_3 (30 wt%), indicating that high dispersion of tungsten oxide species is possibly helpful to the high efficiency of H_2O_2. In addition, it is found that H_2O_2 is partly decomposed into O_2 and H_2O as determined by volumetric measurement.

In order to investigate the stability and duration of active W-species in the W-MCM-48 (20 wt%) catalyst, the leaching of W-species into the product mixture and the left tungsten in the catalyst are also determined after three reaction cycles. No detectable leaching of tungsten species or obvious loss of tungsten in the W-MCM-48 (20 wt%) sample could be found, suggesting the presence of strong interaction between tungsten species and the silica-based matrix with MCM-48 structure. The concentration of the leached out tungsten species from W-MCM-48 (20 wt%) after one reaction cycle is 1.0 ppm in the reaction mixture, suggesting that almost no loss of tungsten in the catalyst could be observed. Results of the selective oxidation of CPE to GA over W-MCM-48 (20 wt%) with different reaction cycles and the regeneration one are listed in Table 5. The GA yield decreases tardily and still keeps above 61% after the third cycle. Moreover, the catalyst can be easily regenerated to its initial high performance after a simple treatment. For the purpose of comparison, Table 5 also gives the catalytic results over the WO_3/SiO_2 (20 wt%) counterpart. It can be seen that the CPE conversion obviously decreases over WO_3/SiO_2 and the GA yield is only 19.2% after three cycles of the reaction. The concentration of the leached out tungsten species from WO_3/SiO_2 (20 wt%) after one reaction cycle is 138 ppm in the reaction mixture, indicating that ca. 8% WO_3 was leached out. This value is much higher than that of W-MCM-48 (20 wt%). Thus, it is not surprising that obvious decrease in the WO_3 content in the WO_3/SiO_2 catalyst is found after three cycles of reaction. In addition, the regenerated catalyst cannot show its initial activity; only 21% of the GA yield is achieved. Therefore, it can be concluded that the interaction between tungsten oxide species and the silica-based matrix of W-MCM-48 by the in situ method is much stronger than that of WO_3/SiO_2 by the impregnated method.

In addition, another experiment has been carried out to test whether this novel W-MCM-48 catalyst is actually heterogeneous. After the reaction over the W-MCM-48 catalyst has been carried out for 10 h, the catalyst is removed through simple filtration and the reaction solution is stirred for another 14 h. No detectable increase in GA yield and CPE conversion in the next 14 h of reaction are observed, indicating that the

Table 5
Reusability and regeneration of 20% W-MCM-48 and 20% WO_3/SiO_2[a]

Catalyst	Entry	H_2O_2 conversion (%)	CPE conversion (%)	GA yield (%)	GA selectivity (%)
20% W-MCM-48	1	98.9	85.2	66.9	78.5
	2	89.9	83.3	64.6	77.6
	3	89.3	82.0	61.4	74.9
	4[b]	93.6	85.1	66.6	78.3
20% WO_3/SiO_2	1	65.2	50.2	30.5	60.8
	2	53.3	41.9	24.1	57.5
	3	43.2	35.2	19.2	54.5
	4[b]	46.6	38.8	21.0	54.2

[a] Reaction conditions: 5 mL cyclopentene, 7 mL 50% H_2O_2, 50 mL *t*-BuOH, 0.1 g WO_3, T = 308 K, reaction time 35 h; CPE, cyclopentene; CPO, cyclopentene-epoxide; GA, glutaraldehyde; CPDL, cyclopentan-1,2-diol; CPLE, 2-*t*-butyloxy-1-cyclopentanol.
[b] After regenerated with heat treatment at 873 K for 3 h.

trace amount of leached W species has almost no detectable catalytic influence on the reaction.

4. Conclusions

In this work, W-containing MCM-48 has been synthesized under hydrothermal conditions via pH adjustment using TEOS as Si source, Na_2WO_4 as W source and CTAB as the structure-directing template. XRD patterns, FT-IR spectra and UV–vis DRS spectra all prove that tungsten has been incorporated into the MCM-48 framework uniformly. The as-synthesized material shows typical structure of MCM-48. WO_3 species are highly dispersed into the lattice of the bulk and might be imbedded separately, which could be served as the active centers for the selective oxidation of CPE to GA. The FT-IR-pyridine adsorption has confirmed the presence of strong Brønsted acid sites and Lewis acid sites upon incorporating tungsten oxide species into the MCM-48 materials, which are beneficial to the catalytic performance. The optimal tungsten content is 20 wt% and the GA yield over this catalyst exceeds 66%, higher than those over commercial and xerogel silica supported WO_3 catalyst or WO_3/TiO_2-SiO_2 catalyst, suggesting its promising potential use in industry.

Acknowledgments

This work was financially supported by the Major State Basic Resource Development Program (Grant No. 2003CB615807), NSFC (Project 20407006, 20473021), the Natural Science Foundation of Shanghai Science & Technology Committee (02DJ14021) and the Committee of the Shanghai Education (02SG04).

References

[1] J.C. Vartuli, K.D. Schmitt, C.T. Kresge, W.J. Roth, M.E. Leonowicz, S.B. McCullen, S.D. Hellring, J.S. Beck, J.L. Schlenker, D.H. Olson, E.W. Sheppard, Chem. Mater. 6 (1994) 2317.
[2] J.S. Beck, J.C. Vartuli, W.J. Roth, M.E. Leonowicz, C.T. Kresge, K.D. Schmitt, C.T.-W. Chu, D.H. Olson, E.W. Sheppard, S.B. McCullen, J.B. Higgins, J.L. Schlenker, J. Am. Chem. Soc. 114 (1992) 10834.
[3] C.T. Kresge, M.E. Leonowicz, W.J. Roth, J.C. Vartuli, J.S. Beck, Nature 359 (1992) 710.
[4] Q.N. Le, R.T. Thomson, Mobil Co. U.S. Patent, US-A 5191144, 1993.
[5] P.J. Branton, P.G. Hull, K.S.W. Sing, J. Chem. Soc. Chem. Commun. 16 (1993) 1257.
[6] A. Corma, Chem. Rev. 97 (6) (1997) 2373.
[7] X. Auvray, C. Petipas, R. Anthore, I. Rico, A. Lattes, J. Phys. Chem. 93 (1989) 7458.
[8] J.M. Kim, S.K. Kim, R. Ryoo, Chem. Commun. 2 (1998) 259.
[9] P. Van Der Voort, M. Mathieu, F. Mees, E.F. Vansant, J. Phys. Chem. B 102 (1998) 8847.
[10] O. Collart, P. Van Der Voort, E.F. Vansant, D. Desplantier, A. Galarneau, F. Di Renzo, F. Fajula, J. Phys. Chem. B 105 (2001) 12771.
[11] M. Kruk, M. Jaroniec, R. Ryoo, J.M. Kim, Chem. Mater. 11 (1999) 2568.
[12] T. Tatsumi, K.A. Koyano, J. Porous Mater. 6 (1999) 13.
[13] Ch. Danumah, S. Vaudreuil, L. Bonneviot, M. Bousmina, S. Giasson, S. Kaliaguine, Microporous Mesoporous Mater. 44–45 (2001) 241.
[14] M. Chatterjee, Y. Ikushima, F.Y. Zhao, New J. Chem. 27 (2002) 510.
[15] M. Kaneda, T. Tsubakiyama, A. Carlsson, Y. Sakamoto, T. Ohsuna, O. Terasaki, J. Phys. Chem. B 106 (2002) 1256.
[16] H. Yoshitake, T. Yokoi, T. Tatsumi, Chem. Mater. 15 (2003) 1713.
[17] K. Morishige, N. Tateishi, S. Fukuma, J. Phys. Chem. B 107 (2003) 5177.
[18] J. Parmentier, C. Vix-Guterl, P. Gibot, M. Reda, M. Ilescu, J. Werckmann, J. Patarin, Microporous Mesoporous Mater. 62 (2003) 87.
[19] I. Díaz, J. Pérez-Parientea, O. Terasaki, J. Mater. Chem. 14 (2004) 48.
[20] S.H. Han, J. Xu, W.G. Hou, X.M. Yu, Y.S. Wang, J. Phys. Chem. B 108 (2004) 15043.
[21] Ch. Subrahmanyam, B. Viswanathan, T.K. Varadarajan, J. Mol. Catal. A 226 (2005) 155.
[22] R.K. Rana, B. Viswanathan, Catal. Lett. 52 (1998) 259.
[23] Z.R. Zhang, J.S. Sue, X.M. Zhang, S.B. Li, Chem. Commun. 2 (1998) 241.
[24] W.L. Dai, H. Chen, Y. Cao, H.X. Li, S.H. Xie, K.N. Fan, Chem. Commun. 7 (2003) 892.
[25] K. Schumacher, C.D. von Hohenesche, K.K. Unger, R. Ulrich, A. Du-Chesne, U. Wiesner, H.W. Spiess, Adv. Mater. 11 (1999) 1194.
[26] A.A. Romero, M.D. Alba, J. Klinowski, J. Phys. Chem. B 102 (1998) 123.
[27] J. Xu, Z.H. Luan, M. Hatrmann, L. Kevan, Chem. Mater. 11 (1999) 2928.
[28] O. Collart, P. Cool, P. Van Der Voort, V. Meynen, E.F. Vansant, K. Houthoofd, P.J. Grobet, O.I. Lebedev, G.V. Tendeloo, J. Phys. Chem. B 108 (2004) 13905.
[29] S. Gómez, O. Giraldo, L.J. Garcés, J. Villegas, S.L. Suib, Chem. Mater. 16 (2004) 2411.
[30] W. Zhao, Y.F. Luo, P. Deng, Q.Z. Li, Catal. Lett. 73 (2001) 199.
[31] M.S. Morey, G.D. Stucky, S. Schwarz, M. Fröba, J. Phys. Chem. B 103 (1999) 2037.
[32] K.A. Koyano, T. Tatsumi, Chem. Commun. 2 (1996) 145.
[33] T. Tatsumi, K.A. Koyano, N. Igarashi, Chem. Commun. 3 (1998) 325.
[34] M.S. Morey, S. O'Brien, S. Schwarz, G.D. Stucky, Chem. Mater. 12 (2000) 898.
[35] G. Oye, J. Sjoblom, M. Stöcker, J. Disper. Sci. Technol. 21 (2000) 229.
[36] Z. Chang, L. Kevan, Langmuir 18 (2002) 911.
[37] Z.Y. Yuan, O. Luo, J.O. Liu, T.H. Chen, J.Z. Wang, H.X. Li, Microporous Mesoporous Mater. 42 (2001) 289.
[38] M. Mathieu, P. Van Der Voort, B.M. Weckhuysen, R. Rao, G. Catana, R.A. Schoonheydt, E.F. Vansant, J. Phys. Chem. B 105 (2001) 3393.
[39] Z.X. Chang, R.M. Krishna, J. Xu, R. Koodali, L. Kevan, Phys. Chem. Chem. Phys. 3 (2001) 1699.
[40] M.S. Morey, J.D. Bryan, S. Schwarz, G.D. Stucky, Chem. Mater. 12 (11) (2000) 3435.
[41] Y.J. Zhang, S.L. Zhao, G.D. Sun, Z.L. Wang, Chin. J. Catal. 21 (4) (2000) 345.
[42] S.P. Gorman, E.M. Scott, A.D. Russell, J. Appl. Bacteriol. 48 (1980) 161.
[43] F.M. Collins, J. Appl. Bacteriol. 61 (3) (1986) 247.
[44] H. Furukawa, F. Nishikawa, T. Koyama, Japanese Patent 6,219,548, 1987.
[45] J.F. Deng, X.H. Xu, H.Y. Chen, A.R. Jiang, Tetrahedron 48 (1992) 3503.
[46] W.Z. Weng, M.S. Chen, Q.G. Yan, T.H. Wu, Z.S. Chao, Y.Y. Liao, H.L. Wan, Catal. Today 63 (2000) 317.
[47] R.H. Jin, H.X. Li, J.F. Deng, J. Catal. 203 (2001) 75.
[48] R.D. Shannon, C.T. Prewitt, Acta Crystallogr. B 25 (1969) 925.

[49] K.M. Reddy, I. Moudrakovski, A. Sayari, J. Chem. Soc. Chem. Commun. 9 (1994) 1059.
[50] P. Selvam, S.E. Dapurkar, Appl. Catal. A: Gen. 276 (2004) 257.
[51] K.S.W. Sing, D.H. Everett, R.A.W. Haul, L. Mosenu, R.A. Pierotti, J. Rouquerol, T. Siemieniewska, Pure Appl. Chem. 57 (1985) 603.
[52] R. Schmidt, M. Stöcker, M.D. Akporiaye, E.H. Tørstad, A. Olsen, Microporous Mater. 5 (1995) 1.
[53] J.G. Graselli, B.J. Bullkin, Analytical Raman Spectroscopy, Wiley, New York, 1991, p. 352.
[54] A. Stein, M. Fendorf, T.P. Jarvie, K.T. Mueller, A.J. Benesi, T.E. Mallouk, Chem. Mater. 7 (1995) 304.
[55] Y. Wand, O. Zhang, Y. Ohishi, T. Shishido, K. Takehira, Catal. Lett. 72 (2001) 215.
[56] E. Briot, J.-Y. Piquemat, M. Vennat, J.-M. Brégeault, G. Chottard, J.-M. Manoli, J. Mater. Chem. 10 (2000) 953.
[57] O. Klepel, W. Böhlmann, E.B. Ivanov, V. Riede, H. Papp, Microporous Mesoporous Mater. 76 (2004) 105.
[58] R.S. Weber, J. Catal. 151 (1995) 470.
[59] E. Iglesia, D.G. Barton, S.L. Soled, S. Miseo, J.E. Baumgartner, W.E. Gates, G.A. Fuentes, G.D. Meitzner, Stud. Surf. Sci. Catal. 101 (1996) 533.
[60] C.W.F.T. Pistorius, J. Chem. Phys. 44 (1966) 4532.
[61] N. Sharma, M. Deepa, P. Varshney, S.A. Agnihotry, J. Non-Cryst. Solids 306 (2002) 129.
[62] C.Y. Chen, H.-X. Li, M.E. Davis, Microporous Mater. 2 (1993) 17.
[63] H. Chen, W.L. Dai, J.F. Deng, K.N. Fan, Catal. Lett. 81 (2002) 131.
[64] Z.R. Zhang, J.S. Suo, X.M. Zhang, S.B. Li, Appl. Catal. A: Gen. 179 (1999) 11.
[65] B.M. Lok, B.K. Marcus, C.L. Angnell, Zeolites 6 (1986) 185.
[66] C. Martin, P. Malet, G. Solana, V. Rives, J. Phys. Chem. B 102 (1998) 2759.
[67] C. Martin, I. Martin, V. Rives, G. Solana, V. Loddo, L. Palmisano, A. Sclafani, J. Mater. Sci. 32 (1997) 6039.
[68] I.E. Wachs, Catal. Today 27 (1996) 437.
[69] R.H. Jin, X. Xia, W.L. Dai, J.F. Deng, H.X. Li, Catal. Lett. 62 (1999) 201.